Subsurface bending and reorientation of tilted vortex lattices in bulk isotropic superconductors due to Coulomb-like repulsion at the surface

E. Herrera,[1,2] I. Guillamón,[1] J. A. Galvis,[3,4] A. Correa,[5] A. Fente,[1] S. Vieira,[1] H. Suderow,[1]
A. Yu. Martynovich,[6] and V. G. Kogan[6]

[1]*Laboratorio de Bajas Temperaturas y Altos Campos Magnéticos, Departamento de Física de la Materia Condensada, Unidad Asociada UAM/CSIC, Instituto de Ciencia de Materiales Nicolás Cabrera, Instituto de Física de la Materia Condensada, Universidad Autónoma de Madrid, E-28049 Madrid, Spain*

[2]*Departamento de Física, Universidad Nacional de Colombia, Bogotá 111321, Colombia*

[3]*Departamento de ciencias naturales, Facultad de ingenieria y ciencias básicas, Universidad Central, Bogotá 110311, Colombia*

[4]*National High Magnetic Field Laboratory, Florida State University, Tallahassee, Florida 32310, USA*

[5]*Instituto de Ciencia de Materiales de Madrid, Consejo Superior de Investigaciones Científicas, CSIC, E-28049 Madrid, Spain*

[6]*Ames Laboratory, Department of Physics & Astronomy, Iowa State University, Ames, Iowa 50011, USA*

(Received 18 March 2017; revised manuscript received 16 July 2017; published 3 November 2017)

We study vortex lattices (VLs) in superconducting weak-pinning platelet-like single crystals of β-Bi_2Pd in tilted magnetic fields with a scanning tunneling microscope. We show that vortices exit the sample perpendicular to the surface and are thus bent beneath the surface. The structure and orientation of the tilted VLs in the bulk are, for large tilt angles, strongly affected by Coulomb-type intervortex repulsion at the surface due to stray magnetic fields.

DOI: 10.1103/PhysRevB.96.184502

I. INTRODUCTION

Rotation in superfluids and superconductors occurs along lines of quantized vortices oriented perpendicular to the rotation plane. Vortex lines tend to be straight to minimize the energy, but they can bend for a variety of reasons, such as supercurrents, fluctuations, or interfaces. For instance, the vortex liquid phase that appears in cuprate superconductors at high temperatures consists of dynamically fluctuating bent vortices [1]. Bent vortices have been observed in superfluid helium [2] and in Bose-Einstein condensates for a range of angular velocities and condensate shapes [3–5]. However, vortex bending has never been observed directly in a superconductor. Scanning tunneling microscopy (STM) is one of the most powerful tools to view vortices because it shows the vortex lattice at high magnetic fields and in real space. To view bent vortices using STM, one has to create a situation where vortices curve close to the surface. In isotropic superconductors, vortices are expected to exit perpendicular to the surface and should thus be bent when applying tilted magnetic fields [6–8]. Here we study vortices in magnetic fields tilted with respect to the surface of the isotropic superconductor β-Bi_2Pd. We find that the whole vortex lattice bends so that all vortices exit perpendicular to the surface. We also find that the interaction at the sample surface due to stray fields plays a decisive role for the bulk vortex lattice structure.

We study vortex lattices (VLs) at the plane surface of platelet-like single crystals of β-Bi_2Pd with $T_c = 5$ K at low temperatures of $T = 0.15$ K [9,10]. The crystalline lattice is tetragonal, and the Fermi surface has sheets of mixed Bi and Pd orbital characters that lead to a near-isotropic macroscopic behavior [11–13]. Upper critical fields along the basal plane and perpendicular to it differ by barely 25% from $H_{c2,ab} = 0.7$ to $H_{c2,ab} = 0.7$ T (at low temperatures), leading to coherence lengths of $\xi_c = 19$ and $\xi_{ab} = 24$ nm [14,15]. Estimates of the penetration depths from the data on the lower critical field give $\lambda_{ab} = 105$ and $\lambda_c = 132$ nm [14].

II. EXPERIMENT

We use a homebuilt STM attached to the dilution refrigerator inserted in a three-axis vector magnet reaching 5 T in the z direction and 1.2 T for x and y [16,17]. β-Bi_2Pd crystals ($3 \times 3 \times 0.5$ mm^3) are mounted with the c axis along the z direction of the magnet. The other two crystalline orientations with respect to x and y of the magnet are found by scanning the surface with atomic resolution to find the square Bi lattice as outlined in Ref. [15]. We provide the in-plane direction of the magnetic field using the azimuthal angle φ, which gives the angle between the in-plane component of the magnetic field and the x axis of the STM scanning window. Crystal growth is described in Ref. [15]. The surface consists of large atomically flat areas of several hundred nanometers in size, separated by step edges [15]. We use a Au tip cleaned and atomically sharpened *in situ* by repeated indentations onto the Au sample [18]. VL images are obtained by mapping the zero-bias conductance normalized to voltages above the superconducting gap [19]. All measurements are performed at $T = 150$ mK. Data usually are acquired within a field-cooled protocol, although, due to weak pinning of this material, we find the same results when changing the magnetic field at low temperatures. No filtering or image treatment is applied to the conductance maps shown below.

III. RESULTS

A. Vortex bending

Let us consider the vortex core shape at the surface. At $\boldsymbol{H} \parallel \boldsymbol{c}$, the vortex cores of β-Bi_2Pd have a circular shape. The core size is $\approx$24 nm at 0.3 T [20] as shown in Fig. 1 by the white circle. If the vortex in a tilted field would have arrived at the surface being straight without any bending, the expected core shape at the surface would be close to an ellipse with the minor and major semiaxes of 24 and $24/\cos\theta$ nm (θ is the angle between $\boldsymbol{H}$ and $\boldsymbol{c}$). For $\theta = 80^\circ$ we would obtain

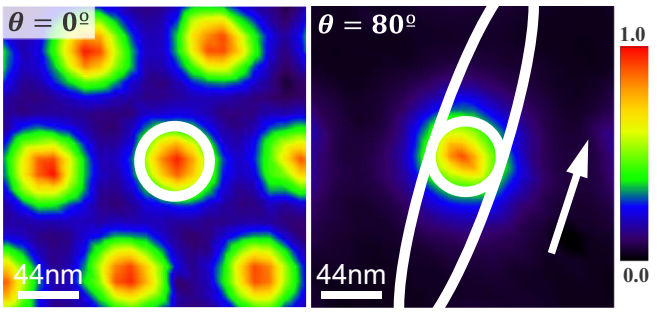

FIG. 1. Zero-bias conductance maps for $H = 0.3$ T, $T = 0.15$ K; $\theta = 0^\circ$ (left) and $\theta = 80^\circ$ (right). The vortex cores in both cases are roughly circles of the same size. The white circles have radii of ~ 24 nm. The white ellipse shows the major semiaxis of $24/\cos\theta$ nm $= 138$ nm. The arrow indicates the tilt direction. The color bar represents the normalized tunneling conductance for both images.

the white ellipse shown in the right panel of Fig. 1. Instead we find the vortex core of the same shape and size as for $\boldsymbol{H}$ normal to the surface as shown by the circle in the right panel of Fig. 1. Thus, our images show that vortices must bend under the surface and exit the sample being perpendicular to the surface.

Vortex bending is expected to occur over a length on the order of the penetration depth $\lambda \approx 100$ nm [6,7,14], which is large relative to the core size of 24 nm. Hence, we do not expect that the electronic density of states at the surface is influenced by the bent part of the vortex deep underneath.

The surface VLs are shown in Fig. 2(a) for a few tilts θ. Panel 2(b) shows that, as expected, the density of vortices at the surface goes as $\cos\theta$.

B. Coulomb-like vortex repulsion at the surface in isotropic superconductors

We now construct a simple model to describe VLs in tilted fields in *isotropic* superconductors. The model predictions, by and large, agree with the STM data. Within this model, the VL in the vortex frame of an infinite sample is hexagonal and *degenerate*: Angle α shown on the left of Fig. 2(c) can be taken as the degeneracy parameter. The circle where all nearest neighbors are located has a radius a fixed by the flux quantization $a^2 = 2\phi_0/\sqrt{3}H$. We use the vortex coordinate frame (x,y,z) with z along the vortex direction and the x axis on the tilt plane. For a given α, the VL unit-cell vectors (in units of a) are

$$\boldsymbol{u}_1 = [\cos\alpha, \sin\alpha],$$
$$\boldsymbol{u}_2 = \left[\cos\left(\alpha + \frac{\pi}{3}\right), \sin\left(\alpha + \frac{\pi}{3}\right)\right]. \quad (1)$$

In a sample much thicker than λ, the VL structure in the bulk is dominated by the bulk interactions, i.e., the VL is still hexagonal. However, the degeneracy of the orientation of the bulk vortex lattice with respect to α can be removed by the intervortex interactions at the surface, particularly for high tilt angles.

To see this, we consider that vortices close to the surface interact mainly through the stray magnetic field. We note that

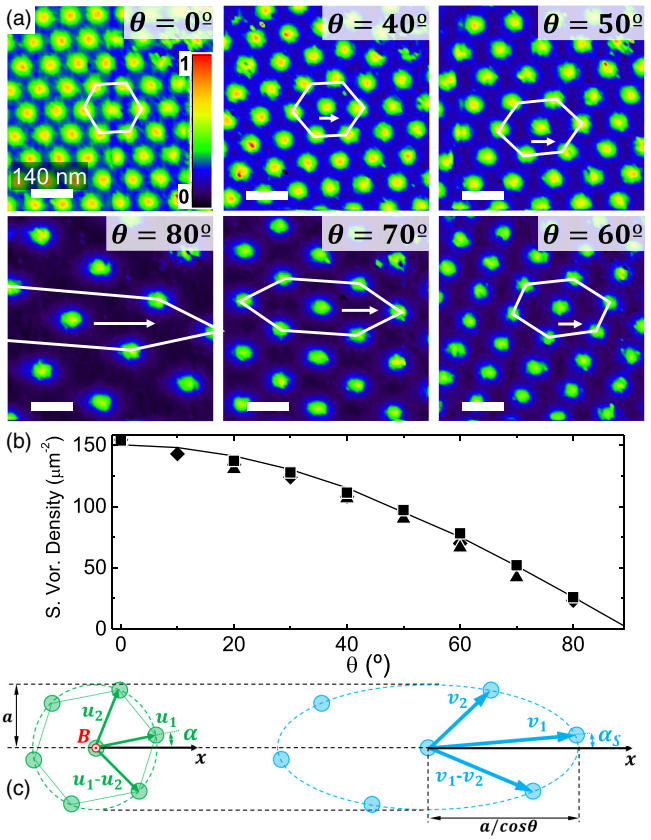

FIG. 2. (a) Zero-bias density of states showing VLs for a few tilt angles θ. The color scale in the top-left panel represents the normalized conductance. The white arrows indicate tilt directions. The white distorted hexagons are projections onto the surface of hexagonal VLs in the bulk. (b) Density of vortices at the surface vs θ and the normal component of the magnetic induction $H\cos\theta$ (solid curve); the different symbols represent different experiments. We use large fields so that the difference between the applied field $\boldsymbol{H}$ and the magnetic induction $\boldsymbol{B}$ can be disregarded. (c) Schematic of the bulk VL in the vortex frame (left panel) with lattice vectors u_1 and u_2 and its surface projection (right panel) with lattice vectors v_1 and v_2 for the tilt along x.

due to subsurface bending the point of the vortex exit is shifted relative to the exit point extrapolated by straight lines following the bulk vortex lattice. In small fields when the vortices are well separated, each one will experience the same shift. We assume that shifts are the same also in fields of our interest. In particular, this implies that the density of bent vortices at the surface is the same as if vortices were straight; this is consistent with the macroscopic boundary condition for the normal component of the magnetic induction $H\cos\theta$. Hence, the arrangement of vortices at the surface is just shifted relative to the VL which would have been there without subsurface bending. Then, considering the VL structure, one can disregard the bending, and the bulk nearest neighbors will be situated at the cross section of a circular cylinder of radius a with the flat surface, i.e., at the ellipse with semiaxes $a/\cos\theta$ and a, in the right panel of Fig. 2(c). Taking again the x axis of the surface frame on the tilt plane, one obtains new unit-cell vectors at the

surface (in units of a),

$$\boldsymbol{v}_1 = \left[\frac{\cos\alpha}{\cos\theta}, \sin\alpha\right],$$
$$\boldsymbol{v}_2 = \left[\frac{\cos(\alpha+\pi/3)}{\cos\theta}, \sin\left(\alpha+\frac{\pi}{3}\right)\right]. \quad (2)$$

In particular, angle α_s between $\boldsymbol{v}_1$ and $\hat{\boldsymbol{x}}$ is related to the parameter α by $\tan\alpha_s = \tan\alpha \ \cos\theta$. All vortex positions at the surface $\boldsymbol{R}_{mn} = m\boldsymbol{v}_1 + n\boldsymbol{v}_2$ (m,n are integers) can be expressed in terms of θ and α (or α_s).

We can now treat the stray fields out of the sample as created by point "monopoles" producing the magnetic flux ϕ_0 in the free space within the solid angle 2π. The interaction energy of the vortex at the origin with the rest is

$$\frac{\phi_0^2}{4\pi^2}\sum_{m,n}{}' \frac{1}{R_{mn}}, \quad (3)$$

where $\sum'$ is over all m,n except $m = n = 0$. The surface vortex density is $H\ \cos\theta/\phi_0$ so that surface interaction per cm^2 is

$$F_s = \frac{\phi_0 H\cos\theta}{4\pi^2}\sum_{m,n}{}' \frac{1}{R_{mn}} = \frac{3^{1/4}\phi_0^{1/2}H^{3/2}}{4\sqrt{2}\pi^2}S(\alpha,\theta), \quad (4)$$

$$S = \cos^2\theta\sum_{m,n}{}'\{[m\ \cos\alpha + n\ \cos(\alpha+\pi/3)]^2 + \cos^2\theta[m\ \sin\alpha + n\ \sin(\alpha+\pi/3)]^2\}^{-1/2}. \quad (5)$$

It readily is checked that $\partial S/\partial\alpha = 0$ at $\alpha = -\pi/6$ and $\pi/3$. The corresponding structures in the vortex frame are hexagons, called hereafter A and A'; in A two out of six nearest neighbors are on the y axis, and in A' they are on the x axis.

The sum S is divergent and as such depends on the summation domain. We, however, are interested only in the angular dependence of $S(\alpha)$ because of its role in removing the VL degeneracy in the bulk. The angular dependence arises mostly due to vortices in the vicinity of the central one because the number of far-away vortices grows with the distance and their combined contribution to the interaction is nearly isotropic. Our strategy for the evaluation of $S(\alpha)$ is based on the fact that the Coulomb interaction out of the sample is isotropic and therefore we can perform the summation within a circle $R_{mn} < L$, where L is large enough to include a few "nearest-neighbor shells" of vortices surrounding the one at the origin. To provide a smooth truncation we add a factor $e^{-R_{mn}^2/L^2}$ to the summand of Eq. (5).

Results of these calculations are given in Fig. 3 for $\theta \approx 80^\circ$, 70°, and 60°; smaller tilt angles are discussed in the Appendix. Clearly, the structure A ($\alpha = -\pi/6$) is unstable. The minimum energy for $\theta = 70^\circ$ and 60° is at $\alpha = 0$ so that the preferred structure is A'. For $\theta = 80^\circ$ the minimum is shifted to $\alpha \approx -0.1$. These qualitative conclusions do not change if one takes a larger radius L of the summation domain, notwithstanding the increase in the calculated surface energy F_s.

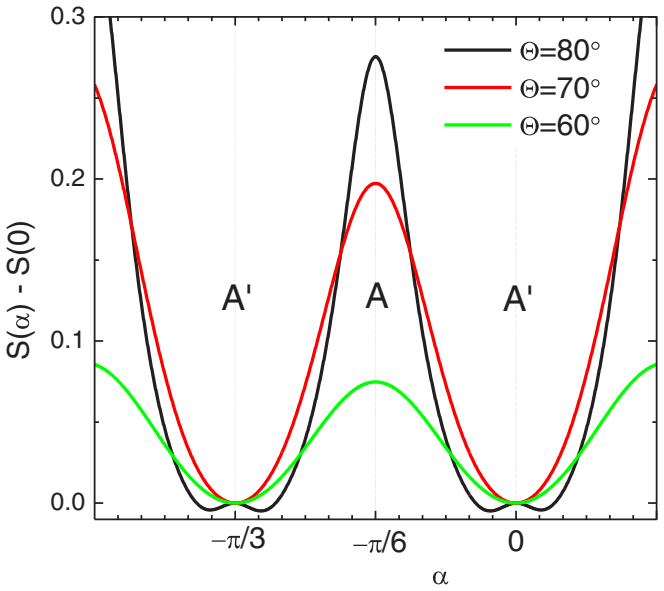

FIG. 3. The surface energy angular dependence $S(\alpha) - S(0)$ for $\theta = 80^\circ$ (black curve), 70° (red curve), and 60° (green curve) for $L = 4$ and $-15 < m,\ n < 15$. Curves $S(\alpha)$ are shifted vertically to have the same zero value at $\alpha = 0$. The curve $\theta = 80^\circ$ is in fact asymmetric relative to $\alpha = 0$ with the absolute minimum at $\alpha \approx -0.1$.

C. Comparison with experiment and reorientation of the vortex lattice

To show that our model describes the data well, and in particular to check again that the bulk hexagonal VL projects onto the surface as if the vortices were straight, one can follow the bulk nearest neighbors and their surface projections. The six nearest neighbors in the vortex frame correspond to the pairs (m,n),

$$(0,1),\ (1,0),\ (0,-1),\ (-1,0),\ (-1,1),\ (1,-1). \quad (6)$$

At the surface, these pairs mark six vortex positions situated at $\pm\boldsymbol{v}_1$, $\pm\boldsymbol{v}_2$, and $\pm(\boldsymbol{v}_1 - \boldsymbol{v}_2)$, see the sketch in Fig. 2(c). These positions at the surface are not necessarily nearest because, at large tilt angles, they form a strongly stretched hexagon whereas the position (1,1) moves closer to the center.

Let us consider $\theta = 80^\circ$ for which according to Fig. 3 $\alpha \approx -0.1$ and evaluate distances $d_1 = |\boldsymbol{v}_1|$, $d_2 = |\boldsymbol{v}_2|$, and $d_3 = |\boldsymbol{v}_1 - \boldsymbol{v}_2|$. Skipping algebra, we provide formulas for these distances in the Appendix. In units of a we obtain $(d_1,d_2,d_3) = (5.68,3.56,2.63)$. Direct measurements at the corresponding image in Fig. 2(a) give $(d_1,d_2,d_3) \approx (6,3.4,2.4)$ in good agreement with calculated values. Hence, the VL in the bulk bends as a whole when reaching the surface, just shifting the geometric projection of the tilted hexagonal bulk VL onto the surface, and loses its degeneracy by arranging with angle α that minimizes the interaction due to stray fields.

In Fig. 4 we show α for experiments changing the in-plane direction of the magnetic field (for a tilt of $\theta = 80^\circ$). We observe that the orientation fluctuates around A'. The deviations from A' can be caused by vortex pinning or by the tetragonal symmetry of the crystalline lattice, not included in our model.

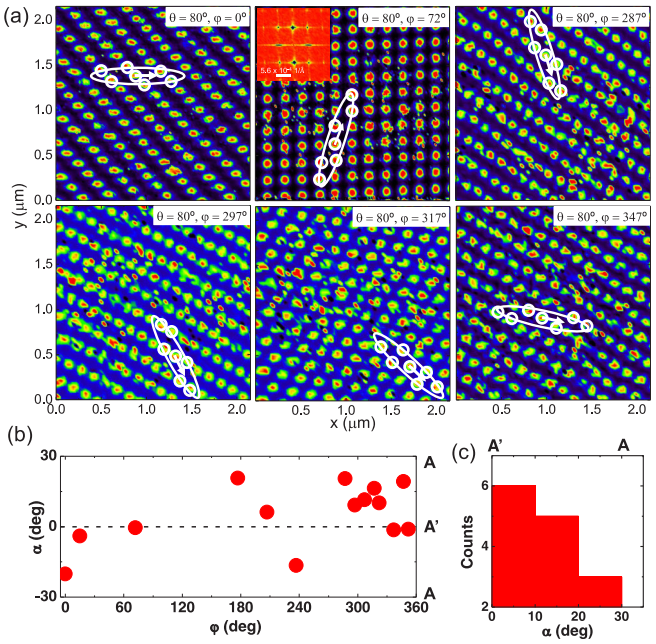

FIG. 4. In (a) we show VLs for a fixed tilt of $\theta = 80^\circ$ but different directions of the in-plane component of the magnetic field, characterized by azimuthal angles φ. VLs are made of vortices strongly bent under the surface. Note that these lattices are still very well ordered, despite the vortex bending. The color scale is the same as in Figs. 1 and 2. In (b) we show angle α [defined in Fig. 2(c)] obtained for images made at a polar angle of $\theta = 80^\circ$ as a function of φ. In (c) we accumulate the absolute values of α in three ranges from low α, close to the A' orientation, to higher α, close to the A orientation.

IV. DISCUSSION

As shown in previous work, VLs in β-Bi_2Pd in fields along c are hexagonal up to H_{c2} with one of the VL vectors along a or b of the tetragonal crystal [15]. This gives a twofold degeneracy in the VL orientation [21] with domains of differently oriented VLs. In some tetragonal materials in fields along c, the fourfold-symmetric nonlocal corrections to the London theory modify the isotropic repulsion and lead to two degenerate rhombic VLs, which at large fields transform to the square VL [22,23]. One of the requirements for the nonlocal corrections to work is a large Ginzburg-Landau parameter κ [24]. In our crystals, $\kappa \sim 4$, and we do not observe VL transitions. Interestingly, at highly tilted fields, the surface intervortex interaction is strong enough to remove the degeneracy observed in fields along c between the two vortex lattice orientations and fix the degeneracy parameter α such that the surface interaction energy is minimized.

We recall that materials with extreme anisotropies, such as $Bi_2Sr_2CaCu_2O_\delta$ reveal Josephson vortex lattices crossing with lattices of two-dimensional pancake vortices. Lorentz microscopy on vortices pinned to columnar defects that were tilted with respect to the surface (the magnetic field being applied perpendicular to the surface) have been studied in $Bi_2Sr_2CaCu_2O_\delta$ [25]. Elongated images with a contrast decreased with respect to perpendicular vortices are found when pinning of pancake vortices to the tilted columnar defects is strong. Further measurements in tilted magnetic fields in the same system show crossing Josephson and pancake vortex lattices, chain vortices, kinked structures of pancakes, as well as flux cutting in nonequilibrium situations [26–32]. On the other hand, measurements in high-purity Nb crystals in tilted magnetic fields show that the bulk VL has a variety of structural transitions, including twofold structures breaking the crystalline fourfold rotation symmetry and scalene unit cells [33]. The Ginzburg-Landau $\kappa \sim 1$ and the observed structures probably show anisotropic features of the Fermi surface of Nb [33]. Tilted VLs have also been studied in 2H-$NbSe_2$, showing distorted hexagons whose orientations disagree with theoretical expectations [34–39]. It was proposed that vortex-induced strain of the crystal might explain the data [40]. At high tilt angles, buckling transitions produce superlattices with chainlike vortex arrangements [36,37]. Besides, vortex cores have starlike shapes in fields along c and acquire cometlike tails in tilted fields, making it difficult to find the vortex core size in this material. The anisotropy in all these materials ranges from the highly anisotropic pancake vortex situation of the cuprates to the isotropic vortices of Nb, passing through the intermediate situation of 2H-$NbSe_2$. No true vortex bending has been seen in these systems either because the bending scale is as short as the interlayer spacing in highly anisotropic systems with pancake vortices or because other effects, such as the influence of the anisotropy of the Fermi surface, have been considered. Our paper shows that the way vortex cores behave close to the surface can be relevant in every situation in tilted fields and contributes to the vortex interactions in the bulk.

To summarize, we have studied VLs in tilted fields in the isotropic superconductor β-Bi_2Pd. We demonstrate that vortices exit the sample being perpendicular to the surface, which necessitates the subsurface bending of vortex lines. We find that intervortex Coulomb-like repulsion at the surface due to stray fields removes the degeneracy of the bulk hexagonal VLs thus fixing the bulk VL orientation.

ACKNOWLEDGMENTS

The authors are grateful to P. C. Canfield for discussions, for having proposed the growth of single crystals of β-Bi_2Pd, and for having shown how to do that. E.H. was supported by the Departamento Administrativo de Ciencia, Tecnología e Innovación, COLCIENCIAS (Colombia) Programa Doctorados en el Exterior Convocatoria Program No. 568-2012 and the Universidad Nacional de Colombia, División de Investigación y Extensión sede Bogotá (DIEB) Project No. 35615. I.G. was supported by the ERC (Grant Agreement No. 679080 and the Ramón y Cajal Program through Grant No. RyC-2014-15093). This work also was supported by the Spanish MINECO (Grants No. FIS2014-54498-R and No. MAT2014-52405-C2-02), by the Comunidad de Madrid through Program NANOFRONTMAG-CM (Program No. S2013/MIT-2850), and by Axa Research Funds. We also acknowledge the SEGAINVEX workshop of UAM, Banco Santander and COST Grant No. CA16128 action, the EU through Grant Agreements No. FP7-PEOPLE-2013-CIG 618321 and No. 604391, and Nanopyme Grant No. FP7-NMP-2012-SMALL-6 NMP3-SL 2012-310516. V.G.K. was supported by the U.S.

Department of Energy, Office of Science, Basic Energy Sciences, Materials Sciences and Engineering Division. The Ames Laboratory is operated for the U.S. DOE by Iowa State University under Contract No. DE-AC02-07CH11358.

APPENDIX

1. Vortex lattices at the surface

Within the *isotropic* model, the VL in the vortex frame of an infinite sample is hexagonal and *degenerate*: Angle α shown in the left panel of Fig. 2(c) can be taken as the degeneracy parameter. For a given α, the VL unit-cell vectors (in units of a) are given by Eq. (1). Positions of the nearest neighbors are $\pm\boldsymbol{u}_1$, $\pm\,\boldsymbol{u}_2$, and $\pm(\boldsymbol{u}_1-\boldsymbol{u}_2)$, and all of them are at the same distance $d=1$ from the vortex at the origin.

It is argued in the main text that, considering the VL structure, one can disregard the vortex bending. Then, the bulk nearest neighbors will be situated at the cross section of a circular cylinder of radius a with the surface plane, i.e., at the ellipse with semiaxes $a/\cos\theta$ and a [the right panel of Fig. 2(c)]. Taking the x axis of the surface frame on the tilt plane, one obtains new unit-cell vectors at the surface (in units of a) given by Eq. (2).

The positions corresponding to the bulk nearest neighbors are $\pm\boldsymbol{v}_1$, $\pm\,\boldsymbol{v}_2$, and $\pm(\boldsymbol{v}_1-\boldsymbol{v}_2)$. These positions at the surface are not necessarily the nearest. Their distances from the vortex at the origin are $d_1=|\boldsymbol{v}_1|$, $d_2=|\boldsymbol{v}_2|$, and $d_3=|\boldsymbol{v}_1-\boldsymbol{v}_2|$. For these distances one has as follows:

$$d_1^2=\frac{\cos^2\alpha+\cos^2\theta\,\sin^2\alpha}{\cos^2\theta}, \tag{A1}$$

$$d_2^2=\frac{\cos^2(\alpha+\pi/3)+\cos^2\theta\,\sin^2(\alpha+\pi/3)}{\cos^2\theta}, \tag{A2}$$

$$d_3^2=\frac{[\cos(\alpha+\pi/3)-\cos\alpha]^2}{\cos^2\theta}+\left[\sin\left(\alpha+\frac{\pi}{3}\right)-\sin\alpha\right]^2. \tag{A3}$$

We provide in Ref. [41] a code calculating the vortex arrangements that can be expected on the surface, according to these equations.

It is worth mentioning that the VL at the surface is always a strongly distorted hexagon. Accordingly, there can be angles θ at which the surface VL is nearly a square. For instance, we can see that the A' configuration with $\alpha=0.1$ leads to a square surface VL for $\theta=78^\circ$. This can be obtained by considering the vectors $\boldsymbol{s}_1=\boldsymbol{v}_1-\boldsymbol{v}_2$ and $\boldsymbol{s}_2=\boldsymbol{v}_2+(\boldsymbol{v}_2-\boldsymbol{v}_1)$. For $\theta\approx 78^\circ$ these are perpendicular $\boldsymbol{s}_1\cdot\boldsymbol{s}_2=0$. A careful examination of this condition leads to the conclusion that the square lattice can be obtained for $\theta\geqslant 74^\circ$. For $\theta=74^\circ$, the square lattice is obtained at $\alpha=-\pi/12$. With increasing θ, there are two values of α, symmetrically positioned around $\alpha=-\pi/12$ where the square lattice is obtained. The separation between these values of α increases and for $\theta\to 90^\circ$, $\alpha\to 0$ and $-\pi/6$. It is noteworthy that we only observe squarelike lattices when α is small, further supporting that the vortex lattice tends to orient along A' as shown by our model calculations.

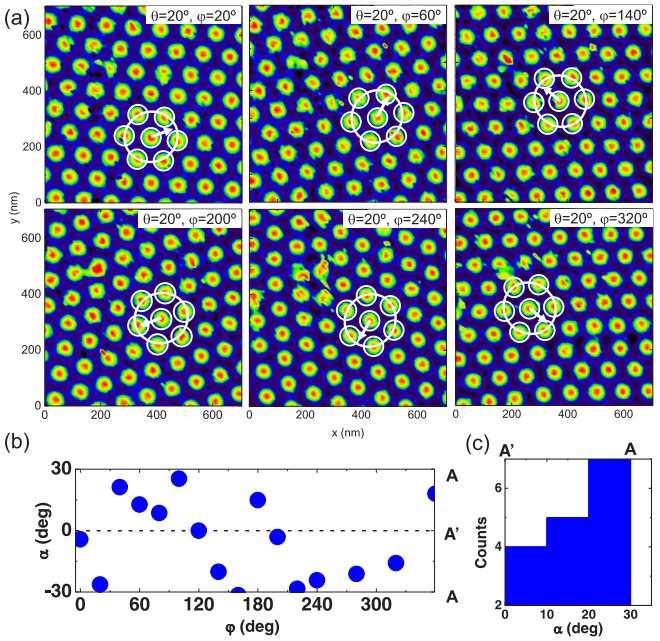

FIG. 5. In (a) we show zero-bias conductance maps for a polar angle of $\theta=20^\circ$ and different in-plane directions of the magnetic field, characterized by azimuthal angles φ. We mark a few vortex hexagons with six white circles. These are joined by white ellipses, following Fig. 2(c). As the polar tilt is so small, the ellipticity hardly is seen in the figure. The white arrows represent the projection of the magnetic field on the plane or φ [counted counterclockwise starting from the positive x axis as shown in Fig. 2(c)]. In (b) we show angle α vs φ. When counting values of α and distributing their absolute values in three angular ranges, we find the histogram shown in (c).

2. Low polar angles

From Fig. 3 one can see that the structure A ($\alpha=-\pi/6$) is unstable since the energy has a maximum at this configuration. Moreover, this feature does not depend on the number of neighbors included in the summation. Hence, we expect that, for relatively small tilts, the minimum energy shown in Fig. 3 corresponds to small α (along with α_S), i.e., the VL structure is close to A'. For $\theta=0.5\approx 28.6^\circ$, the distances d_i are 1.14, 1.04, and 1.04, and all three are larger than 1 as expected because of the Coulomb repulsion. Note that for lattice A, there will be one of the d_i's equal to 1. Thus, even the smallest intervortex distance at the surface exceeds the bulk intervortex distance a.

We now examine experiments for a polar angle $\theta=20^\circ$. The result of the experiment is shown in Fig. 5(a). Here, the vortex lattice remains practically undistorted. In Fig. 5(b) we show α for $\theta=20^\circ$ and different in-plane directions of the magnetic field. As we see in Fig. 5, angle α strongly fluctuates between A and A' with some tendency to orient along A. This suggests that, for this angle, the surface Coulomb interaction is competing with the bulk twofold degeneracy between A and A'. Possibly other effects as the interaction with the crystalline lattice and pinning, which we do not take into account in our model, also play a relevant role.

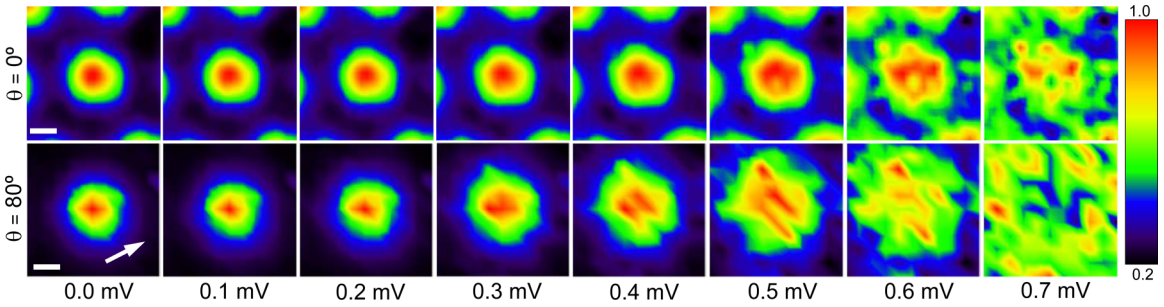

FIG. 6. Conductance map of single vortices for perpendicular fields ($\theta = 0°$, upper row) and strongly tilted magnetic fields ($\theta = 80°$, bottom row). The color scale is given by the bar on the right. The bias voltage for each conductance map is provided in the bottom of the figure. The arrow in the bottom left panel provides the in-plane direction of the magnetic field. The white horizontal bars are of 25 nm.

3. Vortex core shape as a function of the bias voltage

When increasing the bias voltage up from zero bias to the superconducting gap, the vortex core shape slightly changes as discussed in previous work for perpendicular magnetic fields [15,20]. The shape observed in the STM slightly spreads out when reaching the gap edge. This is shown in the top row of Fig. 6. In β-Bi_2Pd, the gap edge is located at about 0.7 mV. The vortex is practically undetectable in conductance maps at bias voltages close to the gap edge because, for this bias voltage just below the gap and when the tunneling conductance is close to its value at high bias voltages, the conductance inside and outside the vortex core is practically the same. For bias voltages below but close to this value, the vortex core shape occupies a larger portion of the image. This is shown in Fig. 6 and has been explained by the superfluid currents around the vortex core. These Doppler shift the gap edge towards slightly lower bias voltages [42–44]. Then, at a distance from the core where the currents are large, the density of states increases for bias voltages just below the gap edge (at, say 0.6 mV), effectively leading to an increased vortex core radius. When the field is nearly parallel, the bias voltage dependence of the vortex core is the same as for perpendicular fields (bottom of Fig. 6). This suggests that the current distribution around the vortex core is not altered by the parallel magnetic field, confirming again vortex bending.

[1] G. Blatter, M. V. Feigel'man, V. B. Geshkenbein, A. I. Larkin, and V. M. Vinokur, Vortices in high-temperature superconductors, Rev. Mod. Phys. **66**, 1125 (1994).

[2] G. P. Bewley, M. S. Paoletti, K. R. Sreenivasan, and D. P. Lathrop, Characterization of reconnecting vortices in superfluid helium, Proc. Natl. Acad. Sci. USA **105**, 13707 (2008).

[3] P. Rosenbusch, V. Bretin, and J. Dalibard, Dynamics of a Single Vortex Line in a Bose-Einstein Condensate, Phys. Rev. Lett. **89**, 200403 (2002).

[4] A. L. Fetter, Rotating trapped Bose-Einstein condensates, Rev. Mod. Phys. **81**, 647 (2009).

[5] J. J. García-Ripoll and V. M. Pérez-García, Vortex bending and tightly packed vortex lattices in Bose-Einstein condensates, Phys. Rev. A **64**, 053611 (2001).

[6] E. H. Brandt, Tilted and curved vortices in anisotropic superconducting films, Phys. Rev. B **48**, 6699 (1993).

[7] A. Martynovich, Magnetic vortices in layered superconducting slabs, Zh. Eksp. Teor. Fis. **105**, 912 (1994).

[8] I. A. Sadovskyy, Y. Jia, M. Leroux, J. Kwon, H. Hu, L. Fang, C. Chaparro, S. Zhu, U. Welp, J.-M. Zuo, Y. Zhang, R. Nakasaki, V. Selvamanickam, G. W. Crabtree, A. E. Koshelev, A. Glatz, and W.-K. Kwok, Toward superconducting critical current by design, Adv. Mater. **28**, 4593 (2016).

[9] Y. Imai, F. Nabeshima, T. Yoshinaka, K. Miyatani, R. Kondo, S. Komiya, I. Tsukada, and A. Maeda, Superconductivity at 5.4 K in $\beta - Bi_2Pd$, J. Phys. Soc. Jpn. **81**, 113708 (2012).

[10] N. Alekseevski, N. Zhuravlev, and I. Lifanov, Zh. Eksp. Teor. Fiz. **125**, 27 (1954).

[11] I. R. Shein and A. L. Ivanovskii, Electronic band structure and fermi surface of tetragonal low-temperature superconductor $\beta - Bi_2Pd$ as predicted from first principles, J. Supercond. Novel Magn. **26**, 1 (2013).

[12] M. Sakano, K. Okawa, M. Kanou, H. Sanjo, T. Okuda, T. Sasagawa, and K. Ishizaka, Topologically protected surface states in a centrosymmetric superconductor $\beta - Bi_2Pd$, Nat. Commun. **6**, 8595 (2015).

[13] A. Coldea (unpublished).

[14] J. Kačmarčík, Z. Pribulová, T. Samuely, P. Szabó, V. Cambel, J. Šoltýs, E. Herrera, H. Suderow, A. Correa-Orellana, D. Prabhakaran, and P. Samuely, Single-gap superconductivity in β-Bi_2Pd, Phys. Rev. B **93**, 144502 (2016).

[15] E. Herrera, I. Guillamón, J. A. Galvis, A. Correa, A. Fente, R. F. Luccas, F. J. Mompean, M. García-Hernández, S. Vieira, J. P. Brison, and H. Suderow, Magnetic field dependence of the density of states in the multiband superconductor $\beta - Bi_2 Pd$, Phys. Rev. B **92**, 054507 (2015).

[16] H. Suderow, I. Guillamón, and S. Vieira, Compact very low temperature scanning tunneling microscope with mechanically driven horizontal linear positioning stage, Rev. Sci. Instrum. **82**, 033711 (2011).

[17] J. A. Galvis, E. Herrera, I. Guillamón, J. Azpeitia, R. F. Luccas, C. Munuera, M. Cuenca, J. A. Higuera, N. Díaz, M. Pazos, M. García-Hernández, A. Buendía, S. Vieira, and H. Suderow, Three axis vector magnet set-up for cryogenic scanning probe microscopy, Rev. Sci. Instrum. **86**, 013706 (2015).

[18] J. G. Rodrigo, H. Suderow, and S. Vieira, Eur. Phys. J. B **40**, 483 (2004).

[19] I. Guillamón, H. Suderow, S. Vieira, L. Cario, P. Diener, and P.

Rodière, Superconducting Density of States and Vortex Cores of 2H − NbS_2, Phys. Rev. Lett. **101**, 166407 (2008).

[20] A. Fente, E. Herrera, I. Guillamón, H. Suderow, S. Mañas-Valero, M. Galbiati, E. Coronado, and V. G. Kogan, Field dependence of the vortex core size probed by scanning tunneling microscopy, Phys. Rev. B **94**, 014517 (2016).

[21] B. Gränz, S. E. Korshunov, V. B. Geshkenbein, and G. Blatter, Competing structures in two dimensions: Square-to-hexagonal transition, Phys. Rev. B **94**, 054110 (2016).

[22] M. R. Eskildsen, K. Harada, P. L. Gammel, A. B. Abrahamsen, N. H. Andersen, G. Ernst, A. P. Ramirez, D. J. Bishop, K. Mortensen, D. G. Naugle, K. D. D. Rathnayaka, and P. C. Canfield, Nature (London) **393**, 242 (1998).

[23] M. Yethiraj, D. K. Christen, D. McK. Paul, P. Miranovic, and J. R. Thompson, Flux Lattice Symmetry in V_3Si: Nonlocal Effects in a High- κ Superconductor, Phys. Rev. Lett. **82**, 5112 (1999).

[24] V. G. Kogan, M. Bullock, B. Harmon, P. Miranović, L. Dobrosavljević- Grujić, P. L. Gammel, and D. J. Bishop, Vortex lattice transitions in borocarbides, Phys. Rev. B **55**, R8693(R) (1997).

[25] A. Tonomura, H. Kasai, O. Kamimura, T. Matsuda, K. Harada, Y. Nakayama, J. Shimoyama, K. Kishio, T. Hanaguri, K. Kitazawa, M. Sasase, and S. Okayasu, Observation of individual vortices trapped along columnar defects in high-temperature superconductors, Nature (London) **412**, 620 (2001).

[26] A. Tonomura, H. Kasai, O. Kamimura, T. Matsuda, K. Harada, T. Yoshida, T. Akashi, J. Shimoyama, K. Kishio, T. Hanaguri, K. Kitazawa, T. Masui, S. Tajima, N. Koshizuka, P. L. Gammel, D. Bishop, M. Sasase, and S. Okayasu, Observation of Structures of Chain Vortices Inside Anisotropic High- T_c Superconductors, Phys. Rev. Lett. **88**, 237001 (2002).

[27] L. N. Bulaevskii, M. Ledvij, and V. G. Kogan, Vortices in layered superconductors with Josephson coupling, Phys. Rev. B **46**, 366 (1992).

[28] S. Bending, Local magnetic pprobe of superconductors, Adv. Phys. **48**, 449 (1999).

[29] A. Tonomura, H. Kasai, O. Kamimura, T. Matsuda, K. Harada, J. Shimoyama, K. Kishio, and K. Kitazawa, Motion of vortices in superconductors, Nature (London) **397**, 308 (1999).

[30] M. Beleggia, G. Pozzi, A. Tonomura, H. Kasai, T. Matsuda, K. Harada, T. Akashi, T. Matsui, and S. Tajima, Model of superconducting vortices in layered materials for the interpretation of transmission electron microscopy images, Phys. Rev. B **70**, 184518 (2004).

[31] A. Buzdin and I. Baladié, Attraction Between Pancake Vortices in the Crossing Lattices of Layered Superconductors, Phys. Rev. Lett. **88**, 147002 (2002).

[32] A. E. Koshelev, Tilted and crossing vortex chains in layered superconductors, J. Low Temp. Phys. **139**, 111 (2005).

[33] S. Mühlbauer, C. Pfleiderer, P. Böni, M. Laver, E. M. Forgan, D. Fort, U. Keiderling, and G. Behr, Morphology of the Superconducting Vortex Lattice in Ultrapure Niobium, Phys. Rev. Lett. **102**, 136408 (2009).

[34] C. A. Bolle, F. De La Cruz, P. L. Gammel, J. V. Waszczak, and D. J. Bishop, Observation of Tilt Induced Orientational Order in the Magnetic Flux Lattice in 2H − $NbSe_2$, Phys. Rev. Lett. **71**, 4039 (1993).

[35] P. L. Gammel, D. A. Huse, R. N. Kleiman, B. Batlogg, C. S. Oglesby, E. Bucher, D. J. Bishop, T. E. Mason, and K. Mortensen, Small Angle Neutron Scattering Study of the Magnetic Flux-Line Lattice in Single Crystal 2H-$NbSe_2$, Phys. Rev. Lett. **72**, 278 (1994).

[36] H. F. Hess, C. A. Murray, and J. V. Waszczak, Scanning Tunneling Microscopy Study of Distortion and Instability of Inclined Flux Line Lattice Structures in the Anisotropic Superconductor 2H − $NbSe_2$, Phys. Rev. Lett. **69**, 2138 (1992).

[37] H. F. Hess, C. A. Murray, and J. V. Waszczak, Flux lattice and vortex structure in 2H − $NbSe_2$ in inclined fields, Phys. Rev. B **50**, 16528 (1994).

[38] I. Fridman, C. Kloc, C. Petrovic, and J. Y. T. Wei, Lateral imaging of the superconducting vortex lattice using doppler-modulated scanning tunneling microscopy, Appl. Phys. Lett. **99**, 192505 (2011).

[39] I. Fridman, C. Kloc, C. Petrovic, and J. Y. T. Wei, Observation of an in-plane vortex lattice transition in the multiband superconductor 2H-NbSe2 using scanning tunneling spectroscopy, arXiv:1303.3559.

[40] V. G. Kogan, L. N. Bulaevskii, P. Miranović, and L. Dobrosavljević-Grujić, Vortex-induced strain and flux lattices in anisotropic superconductors, Phys. Rev. B **51**, 15344 (1995).

[41] https://github.com/LowTemperaturesUAM/Tilted-Vortex-Lattice.

[42] A. Kohen, T. Proslier, T. Cren, Y. Noat, W. Sacks, H. Berger, and D. Roditchev, Probing the Superfluid Velocity with a Superconducting Tip: The Doppler Shift Effect, Phys. Rev. Lett. **97**, 027001 (2006).

[43] A. Maldonado, S. Vieira, and H. Suderow, Supercurrent on a vortex core in 2H − $NbSe_2$: Current-driven scanning tunneling spectroscopy measurements, Phys. Rev. B **88**, 064518 (2013).

[44] C. Berthod, Quasiparticle spectra of Abrikosov vortices in a uniform supercurrent flow, Phys. Rev. B **88**, 134515 (2013).